Journal of Inorganic and General Chemistry
ZAAC
Zeitschrift für anorganische und allgemeine Chemie
www.zaac.wiley-vch.de
RESEARCH ARTICLE

DOI: 10.1002/zaac.202500041

Eu(II)-Based Quaternary Chalcogenides with Noncentrosymmetric Structures Stabilized by Site Disorder of d^{10} Metal Cations

Subhendu Jana, Eric A. Gabilondo, Machima Mongkhonratanachai, P. Shiv Halasyamani, and Paul A. Maggard*

Quaternary metal-chalcogenides combining rare-earth cations with late transition metal cations are attracting growing attention for their optical properties, such as for solar energy conversion or second harmonic generation. Synthetic explorations of the II_3-I_2-IV_2-Ch_8 family (II = Eu; I = Cu or Ag; IV = Si, Ch = S or Se) have yielded $Eu_3Ag_2Si_2S_8$ (1) and $Eu_3Cu_{1.08(1)}Si_{2.42(1)}Se_8$ (2). Their structures have been characterized by X-ray diffraction to form in the noncentrosymmetric space group $I\bar{4}3d$ and to exhibit two distinct types of mixed-site occupancies, for the Ag(I) cations in 1 and mixed Cu(I)/Si(IV) cations in 2. In both, the cation disorder occurs to achieve charge balancing with the chalcogenide anions. A high yield of 1 can be achievedwith optical measurements showing indirect and direct band transitions of ≈2.2(1) and ≈2.4(1) eV, respectively. Its second harmonic generation response is found to be relatively strong, approximately 0.9 $AgGaS_2$, confirming its noncentrosymmetric structure. Band structure calculations reveal the valence and conduction band edges stem predominantly from the filled Ag(I)/Cu(I)-based states and empty Si(IV)-based states, respectively, with additional contributions from the chalcogenide anions. Calculation results also show that cation disorder facilitates a reduction in the antibonding interactions between the Ag(I)/Cu(I) d-based and chalcogenide p-based states.

1. Introduction

Nonlinear optical (NLO) materials have wide applications which include but are not limited to military equipment, health care, and remote sensing.[1–3] The most important criterion for a material to exhibit a second harmonic generation (SHG) response is that it should have a noncentrosymmetric structure.[4] Most notably, the synthesis of complex, noncentrosymmetric, metal chalcogenides has been an active area of research for attaining large SHG responses in the mid-infrared (IR) for NLO applications.[5,6] Limitations of current materials, such as $AgGaQ_2$ and $ZnGeP_2$, are their low laser-induced damage threshold values and extensive photon absorption, making them unsuitable for practical uses.[7] Though, $AgGaQ_2$ (Q = S and Se) is commonly selected as a reference material for its NLO properties and to benchmark the SHG activities of other new materials. Ideally, the material should also be stable in air. For example, while γ-$NaAsSe_2$ shows a very large SHG response of ≈75 AGS, it is also unstable in air.[8,9] Within this context, the fortuitously rich structural chemistry of multinary chalcogenides has facilitated the discovery of many promising solid-state candidates for probing SHG properties.

Solid-state compounds containing tetrahedral building motifs are well-known to lead to noncentrosymmetric space groups and a relatively strong SHG response.[10] Tetrahedral motifs can further condense together to form a wide variety of structures, including from zero to three-dimensional structural connectivities and stabilizing diverse new structure types.[11,12] The coinage metals (e.g., Cu and Ag) and tetrels (e.g., Si, Ge, and Sn) mainly exhibit þ1 and þ4 oxidation states, respectively, and are typically coordinated in tetrahedral geometries by the chalcogenide anions.[12–14] These and related studies have focused on the importance of cations with d^{10} electronic configurations, e.g., Cu(I) and Ag(I) cations, in attaining enhanced SHG responses.[15] Thus, much research has focused on the synthesis of multinary chalcogenides incorporating new combinations of coinage metals with tetrahedrally-coordinated tetrel cations. Exploratory synthetic efforts within these chemical systems have unveiled a large chemical family with the general formula of II_3-I_2-IV_2-Q_8 (II = Ba, Eu, Sr, Pb, and Hg; I = Na, Cu, and Ag; and IV = Si, Sn, and Ge) with noncentrosymmetric space groups (e.g., $I\bar{4}3d$).[14,16–19] For example, the Pb(II)-containing compounds exhibit significant site-disorder and SHG activity.[19] Furthermore, new Eu(II)-containing compounds, e.g, $Eu_3Ag_2Ge_2Se_8$, $Eu_3Ag_2Sn_2Se_8$, and $Eu_3Ag_2Sn_2S_8$, have also recently been uncovered from our synthetic investigations and found to exhibit even larger SHG responses as compared to the Ba or Sr analogs.[17] However, the Si-containing analogs

S. Jana, M. Mongkhonratanachai, P. A. Maggard
Department of Chemistry and Biochemistry, Baylor University, Waco, TX 76798, USA
E-mail: Paul_Maggard@baylor.edu
E. A. Gabilondo, P. S. Halasyamani
Department of Chemistry, University of Houston, Houston, TX 77204, USA

Supporting information for this article is available on the WWW under https://doi.org/10.1002/zaac.202500041

of these compounds had not been previously reported or investigated for their crystalline structures and SHG activities.

Described herein, synthetic investigation of the II_3-I_2-IV_2-Q_8 system, for II = Eu, I = Ag or Cu, IV = Si, and Ch = S or Se, yielded two new noncentrosymmetric compounds, $Eu_3Ag_2Si_2S_8$ (1) and $Eu_3Cu_{1.08(1)}Si_{2.42(1)}Se_8$ (2). Prior literature has established that the Cu-containing chalcogenides typically form with the general formula of II-I_2-IV-Ch_4, such as reported for $BaCu_2SiS_4$, $BaCu_2GeSe_4$, and $SrCu_2SiS_4$.[20–22] To the best of our knowledge, 2 is the first Cu-containing chalcogenide exhibiting the II_3-I_2-IV_2-Ch_8 chemical composition. Structural characterization by single crystal X-ray diffraction (SCXRD) demonstrates that both possess partial disordering of the Cu(I)/Ag(I) sites via two distinct pathways which facilitate charge balancing. The optical bandgap was collected for the polycrystalline $Eu_3Ag_2Si_2S_8$ product. Electronic structure calculations were carried out to understand the origin of their optical properties as well as to elucidate features of their chemical bonding that underpin the structural disorder.

2. Experimental Section

2.1. Synthetic Methods

2.1.1. Starting Materials

Single crystals and polycrystalline phases of two new quaternary chalcogenides, $Eu_3Ag_2Si_2S_8$ and $Eu_3Cu_{1.08(1)}Si_{2.42(1)}Se_8$, were synthesized using the following elemental starting materials: Eu pieces (Alfa Aesar, 99.9% purity), Ag powder (Alfa Aesar, 99.99% purity), Si powder (Alfa Aesar, 99.9% purity), S powder (Sigma Aldrich, 99.999% purity), Eu_2O_3 powder (Alfa Aesar, 99.99% purity), Cu powder (Alfa Aesar, 99.99% purity), Se powder (Alfa Aesar, 99.99% purity), and B powder (Beantown Chemical, 99.9% purity).

2.1.2. Single Crystal Synthetic Conditions

Single crystals of $Eu_3Ag_2Si_2S_8$ (1) were obtained from a reaction with the loaded stoichiometric composition containing Eu (69.5 mg, 0.457 mmol), Ag (32.9 mg, 0.305 mmol), Si (8.6 mg, 0.305 mmol), and S (39.1 mg, 1.219 mmol). The reactants were loaded into a carbon-coated fused-silica tube of 6 mm outer diameter (OD) and sealed under vacuum. The reactants were then heated to 1123 K using a 40 K h^1 ramping rate and annealed for 48 h before cooling to room temperature at a rate of 20 K h^1. Yellow, block-shaped crystals of 1 were recovered. Selected crystals were analyzed using a JEOL scanning electron microscopy (SEM) 6010LA and energy-dispersive X-ray (EDX) spectroscopy, indicating the presence of Eu, Ag, Si, and S in the molar ratio of ≈3:2:2:8, shown in Figure S2, Supporting Information. Analogous synthetic efforts to prepare the Cu-containing analog, i.e., $Eu_3Cu_2Si_2Se_8$, by stoichiometric reaction of the Eu, Cu, Si, and Se elements using varying heating profiles failed to yield the targeted compound. Most reactions instead produced orange-colored Eu_2SiSe_4 crystals[23] along with polycrystalline powder. As an alternative approach, the synthesis of $Eu_3Cu_2Si_2Se_8$ was attempted using the boron-chalcogen mixture method.[24,25] All the chemical manipulations for synthesizing $Eu_3Cu_2Si_2Se_8$ crystals were conducted in an ambient atmosphere as the starting materials are air stable: 93.8 mg (0.267 mmol) of Eu_2O_3 powder, 22.6 mg (0.356 mmol) of Cu powder, 10 mg (0.356 mmol) of Si powder, 112.2 mg (1.421 mmol) of Se powder, and 11.5 mg (1.064 mmol) of B powder were loaded into a carbon-coated 8 mm outer diam-eter fused silica tube and flame sealed under vacuum. The reac-tants were heated to 1223 K in 18 h and annealed for 48 h before cooling to 823 K with a 12 K h^1 cooling rate. Subsequently, the furnace was switched off to allow radiative cooling to room temperature. The reaction mainly produced orange crystals of Eu_2SiSe_4, along with a few yellow-colored block-shaped crystals of $Eu_3Cu_{1.08(1)}Si_{2.42(1)}Se_8$ (2). EDX analyses on selected yellow crystals of 2 showed the presence of Eu, Cu, Si, and Se atoms in the molar ratio of ≈3:1.1:2.4:8. The EDX spectrum and elemental mapping of a selected crystal which was used for SCXRD is provided in Figure S3, Supporting Information.

2.1.3. Bulk Synthesis Conditions

A polycrystalline phase of 1 was synthesized using a two-step solid-state synthesis method. A stoichiometric amount of Eu (231.5 mg, 1.524 mmol), Ag (109.6 mg, 1.016 mmol), Si (28.5 mg, 1.016 mmol), and S (130.3 mg, 4.064 mmol) were loaded into a 12 mm OD carbon-coated fused-silica tube inside a glove box and flame sealed under vacuum. The reactants were heated to 1023 K in 16 h and annealed for 60 h before switching off the furnace. The product was then finely ground and pressed into a circular disk of 10 mm diameter using a hydraulic press. The pellet was again sealed under vacuum inside a 12 mm OD fused-silica tube and heated at 823 K for 48 h. The final product exhibited formation of the polycrystalline phase of 1 with a minute amount of secondary phases as judged by room-temperature powder X-ray diffraction (PXRD) data, provided in Figure S1, Supporting Information. Efforts at the high-purity preparation of 2 failed in every synthetic trial, as the reactions predominantly yielded the Eu_2SiSe_4 phase.

2.2. Single Crystal and Powder X-Ray Diffraction

The crystal structures of 1 and 2 were established using room temperature SCXRD characterization methods. The SCXRD data sets of 1 and 2, which had been previously analyzed by EDX methods, were collected using monochromatized Mo-Kα radiation of a Bruker D8 venture and Rigaku XtaLAB Synergy diffractometers, respectively. These were equipped with a photon III mixed mode detector and a HyPix-Arc 100 detector, respectively. Suitable single crystals were fixed onto a transparent loop under viscous Paratone-N oil and mounted on a goniometer head and the intensity data recorded using APEX4 software.[26] The multi-scan method of the SADABS software package[27] was used to correct for absorption. Based on the extinction conditions and the average intensity statistics (|E^2 1|), the noncentrosymmetic I$\bar{4}$3d space group was suggested by the XPREP program[28] and chosen to solve the structures of both 1 and 2 with the use of the SHELXS program[29] implementing direct methods. The initial

solutions provided six crystallographically independent atomic sites in the asymmetric units of the structures, which were then assigned to respective elements based on coordination environments and peak heights. The occupancies, scale factors, atomic positions, extinction corrections, weight corrections, and anisotropic displacement parameters were further refined using the least squares method in SHELXL.[30] For the structure of 1, the final solution provided four fully occupied sites (Eu1, Si1, S1, and S2) along with two partially occupied Ag sites with occupancies of ≈29.5% and ≈70.3% for Ag1 and Ag2, respectively. For the structure of 2, the final solution provided four fully occupied sites (Eu1, Si1, Se1, and Se2), and one mixed Cu1/Si1 site. The mixed Cu1/Si1 site gave refined occupancies of 72(3)% and 28(3)% for Cu1 and Si1, respectively, and a refined formula of $Eu_3Cu_{1.08(1)}Si_{2.42(1)}Se_8$. The SEM data were consistent with this Cu-deficient and Si-enriched structure, as compared to the ideal 3:2:2:8 molar ratio, and thus matched well with the refined composition. The STRUCTURE TIDY program was used to standardize the atomic positions of the final models.[31] The symmetries of the final solved models were checked using PLATON.[32] Structure refinement details, including Wyckoff positions, site symmetries, and occupancies are listed in Table 1–3 and in the Supporting Information.

The polycrystalline sample of 1 was characterized using PXRD at room temperature in ambient atmosphere using a Cu-Kα radiation source of a PANalytical Empyrean X-ray diffractometer. The diffractometer was operated using 45 kV of voltage and 40 mA of current. A 0.013° of step size was used from 5° to 75°.

Table 1. Crystallographic refinement details for the crystal structures of $Eu_3Ag_2Si_2S_8$ (1) and $Eu_3Cu_{1.08(1)}Si_{2.42(1)}Se_8$ (2).

Refinement parameters	1	2[a,c]
Space group	$I\bar{4}3d$	
a [Å]	13.9320(3)	14.3466(3)
V [Å^3]	2704.2(2)	2952.9(2)
Z	8	8
ρ [gm cm^3]	4.803	5.507
μ [mm^1]	17.84	33.98
R(F)[b]	0.017	0.035
$R_w(F_o^2)$	0.034	0.094
S	1.12	1.17
No. of reflections	9439	2240
No. of independent reflections	567	831
δF [e Å^3]	0.59, –0.61	1.51, 1.35
Flack parameter	0.01(2)	0.04(8)

[a]λ = 0.71073 Å, T = 300(2) K. [b]$R(F) = \sum ||F_o| - |F_c|| / \sum |F_o|$ for $F_o^2 > 2\sigma(F_o^2)$. [c]$R_w(F_o^2) = \{\sum [w(F_o^2 - F_c^2)^2] / \sum [w(F_o^2)^2]\}^{1/2}$. For $F_o^2 < 0$, $w = 1/[\sigma^2(F_o^2) + 8.6318P]$ and $w = 1/[\sigma^2(F_o^2) + (0.0333P)^2 + 57.9671P]$ for the crystal structures of 1 and 2, respectively, where $P = (F_o^2 + 2F_c^2)/3$.

2.3. Physical Property Measurements

A Shimadzu UV3600 spectrophotometer was used to record solid-state diffuse reflectance spectra as a function of wavelength for the polycrystalline sample of 1. Powdered $BaSO_4$ was dried and used as a standard reference to record the reflectance data from 1000 nm (1.24 eV) to 250 nm (4.96 eV). The Kubelka–Munk equation ($\alpha/S = (1 - R^2)/2R$) was applied to transform the reflectance data into absorption data. Here R, S, and α are reflectance, scattering coefficient, and absorption coefficient, respectively.[33] The optical bandgap of the polycrystalline $Eu_3Ag_2Si_2S_8$ sample was evaluated using Tauc plots and the following equation[34]

$$(\alpha h\nu)^n = A(h\nu - E_g) \quad (1)$$

where E_g, A, h, and ν are bandgap, proportionality constant, Planck's constant, and the frequency of light, respectively. The value of constant n represents the nature of band transition, with

Table 2. Atomic coordinates, Wyckoff positions, site symmetries, occupancies, and equivalent isotropic displacement parameters for the structure of 1.

Atom	Wyckoff position	Site Symmetry	x	y	z	U_{eq}	Occupancy
Eu1	24d	2..	0.02232(3)	0	1/4	0.0246(2)	–
Ag1	24d	2..	0.2684(4)	0	1/4	0.073(2)	0.295(4)
Ag2	12a	4..	0.375000	0	1/4	0.0344(6)	0.703(5)
Si1	16c	.3.	0.2348(1)	0.2348(1)	0.2348(1)	0.0130(5)	–
S1	48e	1	0.0856(1)	0.0989(1)	0.4363(1)	0.0160(3)	–
S2	16c	.3.	0.1472(1)	0.1472(1)	0.1472(1)	0.0216(6)	–

Table 3. Atomic coordinates, Wyckoff positions, site symmetries, occupancies, and equivalent isotropic displacement parameters for the structure of 2.

Atom	Wyckoff position	Site symmetry	x	y	z	U_{eq}	Occupancy
Eu1	24d	2..	0.01662(8)	0	1/4	0.0232(3)	–
Cu1	12a	4..	3/8	0	1/4	0.031(2)	0.72(3)
Si1	12a	4..	3/8	0	1/4	0.031(2)	0.28(3)
Si2	16c	.3.	0.2286(2)	0.2286(2)	0.2286(2)	0.010(1)	–
Se1	48e	1	0.08076(8)	0.10835(9)	0.43603(9)	0.0136(3)	–
Se2	16c	.3.	0.1389(1)	0.1389(1)	0.1389(1)	0.0224(5)	–

n = 2 and 1/2 representing direct and indirect band transitions, respectively.

A Ho:YAG laser was used to collect the mid-IR SHG data using a wavelength of 2.09 µm and a modified Kurtz–Perry system at room temperature.[35] The sample was finely ground and sieved to a sample of 90–125 µm particle size to record the frequency-doubled output data using a photomultiplier tube. $AgGaS_2$ (AGS) was used as a standard reference versus peak height for the SHG measurement.

An ≈39.4 mg sample of 1 was loaded into a Gelatin capsule to record magnetic susceptibility data as a function of temperature. Measurements were collected from 17 to 300 K using a 10 T magnetic field of a Quantum Design MPMS VSM instrument.

2.4. Electronic Structure Calculations

Electronic structure calculations were performed using density functional theory methods as implemented in the Vienna Ab Initio Simulation Package (VASP; ver. 6.4.2) with the project augmented wave method (PAW).[36,37] The generalized gradient approximation of Perdew–Burke–Ernzerhof was used to model the electron exchange and correlation. An energy convergence criterion of 10^8 eV and an energy cutoff of 400 eV for the plane wave basis set were used in the calculations combined with the PAW pseudopotentials for Eu (5s,5p,6s,4f,5d), Ag (5s,4d), Cu (4s,3d), Si (3s,3p), Se (4s,4p), and S (3s,4p) in their respective structures. Consistent with prior studies,[38] the on-site Coulomb interaction for the Eu 4f orbitals was approximated ass 6 eV in both compounds. The corresponding structure refinements served as the starting models for full geometry relaxations under the respective symmetry constraints until the norms on the atomic forces converged to <0.01 eV $Å^1$. The cation disorder of the Cu and Ag sites in the respective structures was modeled as previously described for this structure type.[39] Spin-polarized densities-of-states (DOS) calculations were performed using an 8 8 8 k-point mesh (total: 75 k-points) for 1 and a 4 4 4 k-point mesh (total: 36 k-points) for 2. The spin-polarized band structures were calculated following the standard k-point path of Γ-H-N-Γ-P-H|P-N|, as determined by Seek-path,[40] with 10 k-point intersections along each Brillouin zone direction. Finally, calculations of the Crystal Orbital Hamilton Populations (COHP) of the pairwise atomic interactions were carried out on the final converged electronic structures using the Local Orbital Suite Towards Electronic Structure Reconstruction (LOBSTER; ver. 5.1.1) program.[41–45]

3. Results and Discussion

3.1. Synthesis and Crystal Structures

Yellow-colored single crystals of the new quaternary complex chalcogenides, 1 and 2, were synthesized at 1123 and 1223 K, respectively, via high-temperature reactions in sealed tubes. The single crystals of both were found to be stable in air for at least ≈30 days. The single-crystal structural refinements showed that both crystallize in the noncentrosymmetric, cubic, space group $I\bar{4}3d$ with unit cell dimensions of a = 13.9320(3) and 14.3466(3) Å, respectively for $Eu_3Ag_2Si_2S_8$ (1) and $Eu_3Cu_{1.08(1)}Si_{2.42(1)}Se_8$ (2) with Z = 8. Both crystallize as derivatives of the parent $Sr_3Ag_2Ge_2Se_8$ structure type.[46] This relatively complex structure type has been described in detail previously,[17,39] as illustrated in Figure 1 and 2. Each is composed of a similar "$[Eu_3Si_2Ch_8]^{2-}$" (Ch = S or Se) substructure, but which differs in the type of Ag(I) or Cu(I)/Si(IV) disorder that occurs to achieve a charge balancing þ2 within their respective substructures. Briefly, each of the Si(IV) cations is coordinated in a distorted tetrahedral geometry by the chalcogenide anions, with sixteen such "$SiCh_4$" motifs packed as in the Li_3Bi structure type. The alignment of these tetrahedral motifs break the inversion symmetry of the structure. For 1, the Si–S distances, Table S2, Supporting Information, range from 2.113(4) to 2.130(2) Å, consistent with analogous distances in Ba_3SiS_5 (2.139(5)–2.175(9) Å),[47] Eu_2SiS_4 (2.112(1)–2.121(1) Å),[48] and $Sr_3Ag_2Si_2S_8$ (2.117(3)–2.135(2) Å).[49] In 2, the Si–Se bond distances range from 2.229(6) to 2.281(2) Å, in agreement with similar distances in $Na_2EuSiSe_4$ (2.246(2)–2.288(2) Å),[50] Eu_2SiSe_4 (2.2536(7)–2.2633(10) Å),[23] and $Ba_4SiSb_2Se_{11}$ (2.270(3)–2.297(3) Å).[51]

The packing of the Eu(II) cations is conserved without disorder in each structure, consisting of $EuCh_8$ (Ch = S, Se) polyhedra with Eu-Ch distances as found in related europium chalcogenide structures.[46,52] Temperature-dependent magnetic susceptibility data are consistent with the Eu(II) cation oxidation state, as given in more detail in the Supporting Information. Taken together with the $SiCh_4$ tetrahedra, a "$[Eu_3Si_2Ch_8]^{2-}$" substructure is formed with Z = 8, i.e., with a formal 16 charge per unit cell. Consequently, the crystallographic sites for the coinage metal Ag(I)/Cu(I) cations in each structure exhibit appreciable site disorder to balance this charge. For the structure of 1, the mixed-site disorder of the Ag(I) cations occurs has been described previously.[17,39] Briefly, the two fractionally occupied Ag sites, Ag1 and Ag2 in Table 2 and in Figure 1, 2b and 3, occur as conjoined polyhedra forming a trimeric "Ag1-Ag2-Ag1" motif with Ag–Ag distances of 1.485(6) Å. Only the Ag1 or Ag2 site could be occupied concurrently. While the occupation of the central Ag2 site is energetically preferred, its Wyckoff site multiplicity of 12 is insufficient to balance the 16 charge on the substructure in the unit cell. Thus, an additional

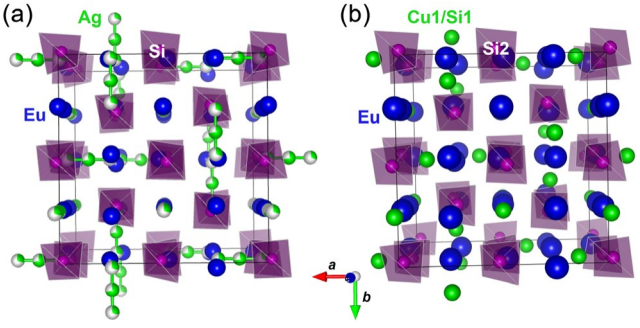

Figure 1. Unit cell views of $Eu_3Ag_2Si_2S_8$ (1; a) and $Eu_3Cu_{1.08(1)}Si_{2.42(1)}Se_8$, (2; b) showing the packing of $SiCh_4$ (Ch = S, Se) tetrahedra (purple) and disordered Ag and Cu1/Si1 sites. Chalcogenide atoms are not drawn for clarity.

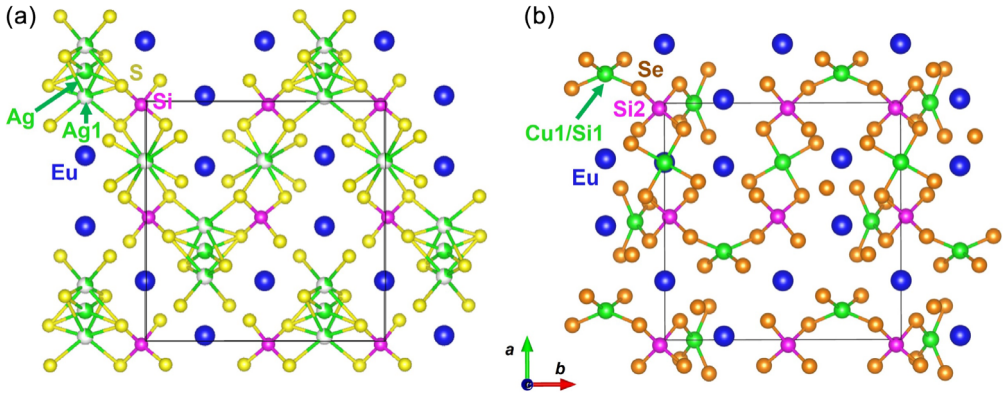

Figure 2. Structural views of single layers of $Eu_3Ag_2Si_2S_8$ (1; a) and $Eu_3Cu_{1.08(1)}Si_{2.42(1)}Se_8$, (2; b) illustrating the two types of disorder for the respective Ag(I) sites and Cu/Su1 sites in each, with atom types and unit cells labeled.

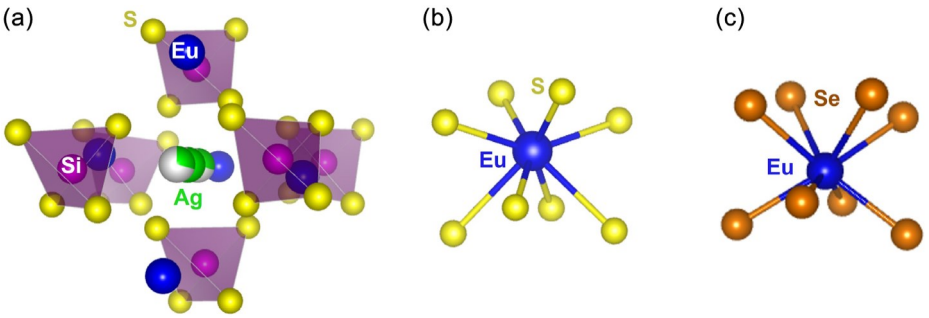

Figure 3. a) View of the channel formed by SiS_4 tetrahedral units in the structure of 1, which are occupied by Ag1, Ag2, and Eu; b,c) the local $EuCh_8$ polyhedra within the structures of 1 and 2.

≈29.5(4)% partial occupation of the Ag1 site with a larger Wyckoff site multiplicity of 24 leads to a closer charge balancing of the substructure, giving a $Eu_3Ag_{1.94(1)}Si_2S_8$ composition which is near to the charge-balanced $Eu_3Ag_2Si_2S_8$ formula.

For the structure of 2, the partial occupation of the Wyckoff site with a larger multiplicity of 24 for the coinage metal is absent. Rather, this compound forms with ≈28(3)% of the Cu(I) sites substituted by Si(IV) at the smaller Wyckoff-site multiplicity of 12, to achieve a closer charge balancing of the "$[Eu_3Si_2Se_8]^{2\prime\prime}$ substructure. Like the isolated "$SiSe_4$" tetrahedra described above, the mixed Cu1/Si1 site is coordinated by the selenide anions in distorted tetrahedral motifs. Condensation between the Cu1/Si1- and Si2-centered tetrahedra in 2 yields an alternative description of a three-dimensional $[Cu_{1.08(1)}Si_{2.42(1)}Se_8]^{5.24}$ network, Figure S6, Supporting Information, that is charge balanced by the Eu(II) cations, Figure 3. The Cu1–Se distances of 2.498(1) Å are consistent with analogous distances in the related structures of $BaScCuSe_3$ (2.4342(4)–2.4532(4) Å)[53] and $BaCuYSe_3$ (2.472(1)–2.528(1) Å).[54] This mixed-site substitution is likely facilitated by the relatively similar ionic radii of the Cu(I) and Si(IV) cations as compared to the more disparate sizes of the Ag(I)/Si(IV) cations in 1. Considering the oxidation states of þ2, þ1, þ4, and –2 for the respective Eu, Cu, Si, and Se atoms in $Eu_3Cu_{1.08(1)}Si_{2.42(1)}Se_8$, there is a small unbalanced charge of þ0.76 per formula. The chemical compositions of crystals of 2 were measured by EDX analyses, Figure S3, Supporting Information, and found to be consistent with the refined composition. The analysis showed Eu, Cu, Si, and Se in the approximate molar ratio of 3:1.1:2.4:8. However, a small percentage of vacancies on the Cu1/Si1 site would lead to a finer charge balancing and cannot be ruled out based on the crystal structure refinement or EDX results. Similar Cu-deficient compounds are frequently found to occur, such as reported for $Ba_2Cu_{7x}Te_6$[55] and $Ba_2Cu_{4x}Te_5$.[56] In addition, mixed-site refinements with partial occupancies in disordered compounds are associated with some errors, especially for nonstoichiometric compounds. For example, excess formal charges of 0.11 and þ0.22 per formula unit have previously been observed in mixed-site compounds such as $Ba_{3.14(4)}Sn_{0.61(1)}Bi_{2.39(1)}S_8$ and $La_3SnFe_{0.61(1)}Se_7$,[57,58] respectively.

3.2. Optical Properties

Solid-state UV–Vis–NIR diffuse reflectance data were measured on the yellow-colored $Eu_3Ag_2Si_2S_8$ (1) powder between a wavelength range of 250 and 1000 nm. The resulting data are given as a Tauc plot, depicted in Figure 4a, for estimation of the optical bandgap and type. The direct and indirect band transitions were calculated to be 2.4(1) and 2.2(1) eV, respectively, consistent with its yellow color and an indirect bandgap. The optical band transitions of 1 are found to be higher in energy than for the

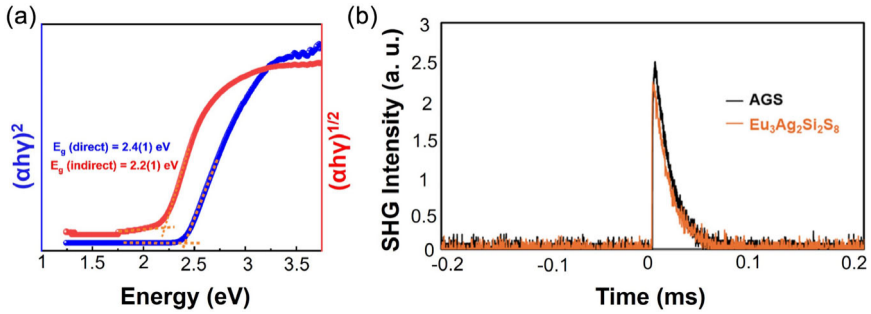

Figure 4. Plotted in a) the Tauc plot of the direct (blue) and indirect (red) band transitions for 1, and b) the SHG responses of the AGS reference sample (black) compared to 1 (orange).

isostructural Eu(II)-containing congeners recently reported, such as for $Eu_3Ag_2Sn_2S_8$ (≈2.2 eV and < 2 eV, direct and indirect, respectively) and $Eu_3Ag_2Sn_2Se_8$ (≈2.1 eV and < 2 eV, respectively).[17] The replacement of the Sn(IV) cation by the lighter Si(IV) cation has had the effect of increasing both types of band transitions by ≈0.2 eV. By comparison, the Ge-analog of $Eu_3Ag_2Ge_2Se_8$ has a similar, direct, band transition of ≈2.4 eV and a wider indirect bandgap of ≈2.0 eV. The trend in the bandgaps generally follows the order of Si(IV) > Ge (IV) > Sn(IV) for the tetrel cations, while the trend with respect to the chalcogenide, i.e., S > Se, was found within this isostuctural series of compounds.

In our previous report,[17] several new members of the isostructural series of Eu(II)-containing chalcogenides ($Eu_3Ag_2Sn_2S_8$, $Eu_3Ag_2Sn_2Se_8$, and $Eu_3Ag_2Ge_2Se_8$) were found to exhibit large SHG responses. The SHG response of a polycrystalline sample of 1 was measured using the modified Kurtz–Perry system and a Ho:YAG laser with a 2.09 µm wavelength. As shown in Figure 4b, the powder of 1 was found to be SHG active and confirming its noncentrosymmetric structure. A comparison of the SHG responses of related metal-chalcogenide structures is listed in Table 4. Although the SHG response of 1 is lower than most of the previously reported series, a it is comparable with the $AgGaS_2$ (AGS) reference.

3.3. Electronic Structure Calculations

Electronic structure calculations were carried out using density functional theory methods to probe the origins of the optical properties of 1 and 2, including the spin-polarized DOS, band structures, and the individual atomic orbital contributions. Full geometry relaxations of both structures were first obtained using the appropriate symmetry constraints of their cubic space group. The results are plotted in Figure 5. The edges of the valence band (VB) and conduction band (CB) of 1 stem predominantly from the spin-polarized Eu $4f^7$-based states and an admixture of empty Si/S (3p)-based states, respectively, in Figure 5a. Conversely, the electronic structure of 2 was modeled with and without the substitution of Si(IV) cations on the Cu(I) sites. Without inclusion of this Cu(I)/Si(IV)-site disorder, i.e., calculated as "$Eu_3Cu_{1.5}Si_2Se_8$", Figure 5b, the Fermi level occurs within the top of the VB comprised of filled Cu d-based states. In essence, this situation would represent an oxidation of Cu(I) cations. However, the incorporation of ≈28% of Si(IV) mixed onto the Cu(I) sites adds electrons and shifts the Fermi level past the top of the VB comprised of filled $3d^{10}$-based Cu states. Concomitantly, the partial DOS contributions of the Cu-based states decrease at the VB edge. The CB edge of 2 is comprised of empty Si/Se (3p/4p)-based states and which are relatively more disperse as compared to the CB edge in 1. In both compounds, the band structures at the VB edges, Figure 5c,d, show relatively flat bands that can be ascribed to the Eu $4f^7$-based states.

The bonding/antibonding characters of the pairwise atomic interactions, e.g., Eu-Se or Si-S, were probed with calculations of the COHP as a function of energy. The results are plotted together in Figure 6, showing bonding (þ) and antibonding () populations of each pairwise interaction with respect to the Fermi level. In both 1 and 2, the unoccupied states above the Fermi level are all increasingly antibonding in nature. The COHPs for the Si-(S/Se) and Eu-(S/Se) interactions are predominantly bonding below the Fermi levels of each compound, with the former occurring at relatively deeper energies as compared to the latter. Conversely, the Ag-S and Cu-Se interactions in 1 and 2, respectively, strongly shift from bonding to antibonding in nature nearer to the Fermi level. This is generally consistent with M(I)-containing compounds with filled d^{10} cations and metal-based antibonding interactions to the near-neighbor ligands. However, substitution of the Cu(I) cations by Si(IV) cations in 2 would act to decrease the Cu-Se antibonding interactions near the Fermi level, thus helping to stabilize this first known example of Cu(I) cations for this structure type. Future investigations are aimed at the synthesis of Cu(I) analogs in high purity for property measurements of their bandgaps and SHG activities.

Table 4. SHG activities in reported isostructural compounds related to $Eu_3Ag_2Si_2S_8$ (1).

Compound	Space group	Bandgap [eV]	SHG (AGS)	Reference
$AgGaS_2$	$I\bar{4}2d$	2.64	1	[60]
$Eu_3Ag_2Si_2S_8$	$I\bar{4}3d$	2.2	≈0.9	This work
$Eu_3Ag_2Sn_2S_8$	$I\bar{4}3d$	<2.0	≈7.0	[17]
$Eu_3Ag_2Sn_2Se_8$	$I\bar{4}3d$	<2.0	≈1.9	[17]
$Eu_3Ag_2Ge_2Se_8$	$I\bar{4}3d$	2.0	≈4.7	[17]
$Sr_3Ag_2Ge_2S_8$	$I\bar{4}3d$	2.62	≈1.3	[14]
$Ba_3CdSn_2S_8$	$I\bar{4}3d$	2.30	≈0.8	[16]
$Hg_3Na_2Ge_2S_8$	$I\bar{4}3d$	2.68	≈3.0	[18]

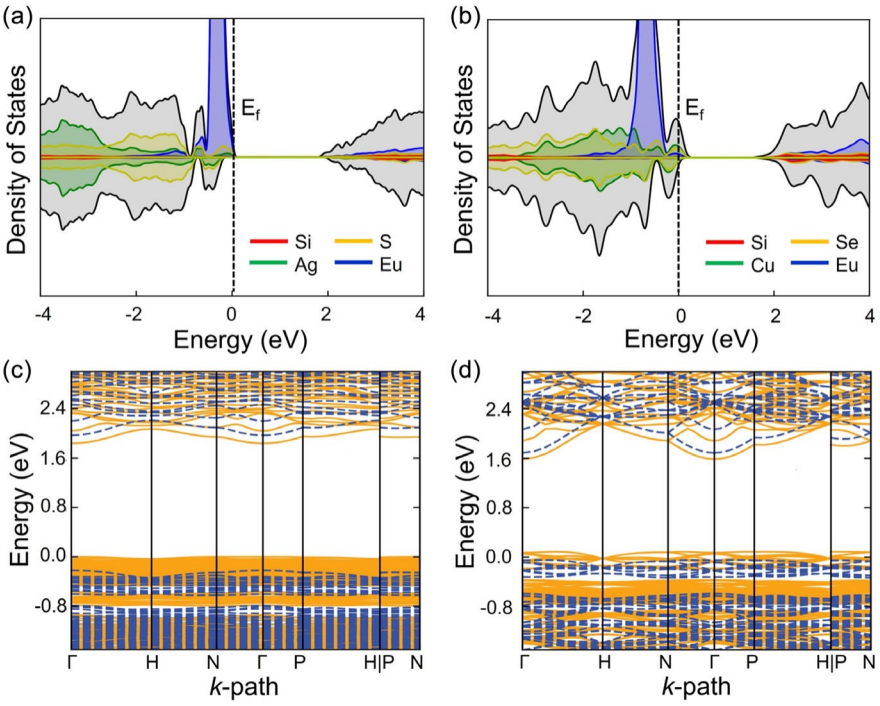

Figure 5. Calculated spin-polarized DOS and band structures for $Eu_3Ag_2Si_2S_8$ (1; a,c)) and $Eu_3Cu_{1.08(1)}Si_{2.42(1)}Se_8$ (2; b,d)) with the Fermi levels (E_f) labeled at 0 eV, the colored lines labeling the atomic orbital contributions and the spin-polarized bands labeled as up (yellow, solid) and down (blue, dashed). The total DOS is represented by black lines with gray shading in panels (a) and (b).

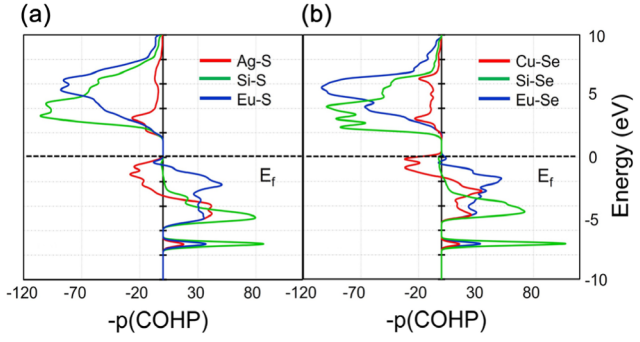

Figure 6. Calculated COHP for the Ag-S, Si-S, and Eu-S interactions for 1 a); $Eu_3Ag_2Si_2S_8$ and the Cu-Se, Si-Se, and Eu-Se interactions for 2 b); modeled as "$Eu_3Cu_{1.5}Si_2Se_8$", with the dashed line indicating the Fermi levels (E_f) in each.

4. Conclusion

Synthetic investigations of quaternary metal chalcogenides combining coinage metal cations with d^{10} electronic configurations with the divalent Eu(II) cation have yielded two new members of the II_3-I_2-IV_2-Ch_8 structural family (II = Eu; I = Cu or Ag; IV = Si, Ch = S or Se), $Eu_3Ag_2Si_2S_8$ (1), and $Eu_3Cu_{1.08(1)}Si_{2.42(1)}Se_8$ (2). Both crystallize in the noncentrosymmetric $I\bar{4}3d$ space group, with 2 representing the first reported Cu-containing chalcogenide exhibiting this chemical composition and structure type. Structural characterization by SCXRD shows that both possess partial disorder over the Cu(I)/Ag(I) sites which facilitates charge balancing of the "$[Eu_3Si_2Ch_8]^{2-}$" (Ch = S or Se) substructures via two distinct pathways. For 1, this occurs with disorder of the Ag atoms over two closely-spaced Wyckoff positions having different multiplicities. For the structure of 2, a substitutional disorder of Cu(I) and Si(IV) occurs on a single Wyckoff site to reach an average oxidation state that facilitates a charge-balanced structure. Both compounds crystallize as yellow-colored powders, with the bandgap and SHG response of 1 measured to be ≈2.2 eV (indirect) and ≈0.9 AGS, respectively. Electronic structure calculations show predominantly antibonding interactions occur between the chalcogenide anions and the Ag/Cu d^{10}-based states for the valence band. For the conduction band, antibonding interactions occur between the chalcogenide anions and the empty Si-based states. This study extends the short list of Eu(II)-containing quaternary chalcogenides known to be potentially suitable as NLO materials.

Acknowledgements

The authors acknowledge primary support of this work from the National Science Foundation (DMR-2317605 and DMR-2516105). This work used the High-Performance Research Computing FASTER cluster at Texas A&M University through allocation CHE240107 from the Advanced Cyberinfrastructure Coordination Ecosystem: Services & Support (ACCESS) program,[59] which is supported by U.S. National Science Foundation grant nos. 2138259, 2138286, 2138307, 2137603, and 2138296. P.S.H. and E.A.G. thank the Welch Foundation (grant E-1457) for support.

Conflict of Interest

The authors declare no conflict of interest.

Data Availability Statement

The data that support the findings of this study are available in the supplementary material of this article.

Keywords: europium chalcogenides · noncentrosymmetric structures · semiconductor · solid-state synthesis

[1] H. D. Tholl, in Technologies for Optical Countermeasures XV, SPIE, Berlin, Germany 2018, p. 1079702.
[2] E. Garmire, Opt. Express 2013, 21, 30532.
[3] X. Luo, Z. Li, Y. Guo, J. Yao, Y. Wu, J. Solid State Chem. 2019, 270, 674.
[4] P. S. Halasyamani, K. R. Poeppelmeier, Chem. Mater. 1998, 10, 2753.
[5] H.-D. Yang, M.-Y. Ran, W.-B. Wei, X.-T. Wu, H. Lin, Q.-L. Zhu, Mater. Today Phys. 2023, 35, 101127.
[6] W. Zhou, S.-P. Guo, Acc. Chem. Res. 2024, 57, 648.
[7] P. G. Schunemann, K. L. Schepler, P. A. Budni, MRS Bull. 1998, 23, 45.
[8] T. K. Bera, J. I. Jang, J.-H. Song, C. D. Malliakas, A. J. Freeman, J. B. Ketterson, M. G. Kanatzidis, J. Am. Chem. Soc. 2010, 132, 3484.
[9] J. He, A. K. Iyer, M. J. Waters, S. Sarkar, R. Zu, J. M. Rondinelli, M. G. Kanatzidis, V. Gopalan, Adv. Opt. Mater. 2022, 10, 2101729.
[10] P. Feng, J.-X. Zhang, M.-Y. Ran, X.-T. Wu, H. Lin, Q.-L. Zhu, Chem. Sci. 2024, 15, 5869.
[11] Y. Yang, K. Wu, B. Zhang, X. Wu, M.-H. Lee, Inorg. Chem. 2020, 59, 2519.
[12] L.-Q. Yang, X.-M. Jiang, S.-M. Pei, W.-F. Chen, B.-W. Liu, G.-C. Guo, ACS Appl. Mater. Interfaces 2022, 14, 4352.
[13] C. Liu, S.-H. Zhou, C. Zhang, Y.-Y. Shen, X.-Y. Liu, H. Lin, Y. Liu, Inorg. Chem. Front. 2022, 9, 478.
[14] Y. Yang, M. Song, J. Zhang, L. Gao, X. Wu, K. Wu, Dalton Trans. 2020, 49, 3388.
[15] J. Cheng, B. Lei, C. Zhou, S. Pan, Z. Yang, Dalton Trans. 2019, 48, 2592.
[16] N. Zhen, K. Wu, Y. Wang, Q. Li, W. Gao, D. Hou, Z. Yang, H. Jiang, Y. Dong, S. Pan, Dalton Trans. 2016, 45, 10681.
[17] S. Jana, E. A. Gabilondo, M. Mongkhonratanachai, Y. Zhang, P. S. Halasyamani, P. A. Maggard, Chem. Mater. 2024, 36, 9750.
[18] K. Wu, Z. Yang, S. Pan, Chem. Mater. 2016, 28, 2795.
[19] J. A. Aitken, G. A. Marking, M. Evain, L. Iordanidis, M. G. Kanatzidis, J. Solid State Chem. 2000, 153, 158.
[20] A. Sarkar, G. Viswanathan, K. Wu, G. J. Miller, K. Kovnir, Z. Anorg. Allg. Chem. 2023, 649, e202300147.
[21] Y. Yang, K. Wu, X. Wu, B. Zhang, L. Gao, J. Mater. Chem. C 2020, 8, 1762.
[22] M. Tampier, D. Johrendt, Z. Anorg. Allg. Chem. 2001, 627, 312.
[23] G. Panigrahi, G. Morrison, M. D. Smith, Inorg. Chem. 2024, 63, 23802.
[24] L. S. Breton, V. V. Klepov, H.-C. zur Loye, J. Am. Chem. Soc. 2020, 142, 14365.
[25] L.-M. Wu, D.-K. Seo, J. Am. Chem. Soc. 2004, 126, 4676.
[26] Bruker APEX4 Version 2009.5-1 Data Collection and Processing Software, Bruker Analytical X-Ray Instruments, Inc., Madison, WI 2009.
[27] G. M. Sheldrick, SADABS, Bruker AXS, Inc., Madison, WI 2008.
[28] G. M. Sheldrick, XPREP Version 2008/2, Bruker AXS Inc., Madison 2018.
[29] G. M. Sheldrick, Acta Cryst. A 2008, 64, 112.
[30] G. M. Sheldrick, Acta Cryst. C 2015, 71, 3.
[31] L. M. Gelato, E. Parthé, J. Appl. Cryst. 1987, 20, 139.
[32] A. L. Spek, J. Appl. Cryst. 2003, 36, 7.
[33] G. Kortüm, Reflectance Spectroscopy: Principles, Methods, Applications, Springer Science & Business Media, New York, NY 2012.
[34] P. Makuła, M. Pacia, W. Macyk, J. Phys. Chem. Lett. 2018, 9, 6814.
[35] S. K. Kurtz, T. T. Perry, J. Appl. Phys. 1968, 39, 3798.
[36] G. Kresse, Phys. Rev. B 1996, 54, 11169.
[37] G. Kresse, Comput. Mater. Sci. 1996, 6, 15.
[38] M. Yu, S. Yang, C. Wu, N. Marom, npj Comput. Mater. 2020, 6, 1.
[39] G. C. McKeown Wessler, T. Wang, V. Blum, D. V. Mitzi, Inorg. Chem. 2022, 61, 2929.
[40] Y. Hinuma, G. Pizzi, Y. Kumagai, F. Oba, I. Tanaka, Comput. Mater. Sci. 2017, 128, 140.
[41] R. Dronskowski, P. E. Bloechl, J. Phys. Chem. 1993, 97, 8617.
[42] V. L. Deringer, A. L. Tchougréeff, R. Dronskowski, J. Phys. Chem. A 2011, 115, 5461.
[43] S. Maintz, V. L. Deringer, A. L. Tchougréeff, R. Dronskowski, J. Comput. Chem. 2016, 37, 1030.
[44] S. Maintz, V. L. Deringer, A. L. Tchougréeff, R. Dronskowski, J. Comput. Chem. 2013, 34, 2557.
[45] R. Nelson, C. Ertural, J. George, V. L. Deringer, G. Hautier, R. Dronskowski, J. Comput. Chem. 2020, 41, 1931.
[46] M. Tampier, Ph.D. Thesis, Heinrich-Heine-Universität in Düsseldorf, Düsseldorf, Germany 2002.
[47] D. Schmitz, Acta Cryst. B 1981, 37, 518.
[48] I. Hartenbach, T. Schleid, Z. Anorg. Allg. Chem. 2002, 628, 1327.
[49] G. C. McKeown Wessler, T. Wang, J.-P. Sun, Y. Liao, M. C. Fischer, V. Blum, D. B. Mitzi, Inorg. Chem. 2021, 60, 12206.
[50] A. Choudhury, P. K. Dorhout, J. Am. Chem. Soc. 2007, 129, 9270.
[51] K.-S. Choi, M. G. Kanatzidis, Inorg. Chem. 2001, 40, 101.
[52] S. Jana, S. O'Donnell, I. A. Leahy, A. Koldemir, R. Pöttgen, R. W. Smaha, P. A. Maggard, J. Mater. Chem. C 2024, 12, 11769.
[53] M. Ishtiyak, S. Jana, R. Karthikeyan, M. Ramesh, B. Tripathy, S. K. Malladi, M. K. Niranjan, J. Prakash, Inorg. Chem. Front. 2021, 8, 4086.
[54] S. Maier, J. Prakash, D. Berthebaud, O. Perez, S. Bobev, F. Gascoin, J. Solid State Chem. 2016, 242, 14.
[55] B. A. Kuropatwa, A. Assoud, H. Kleinke, Inorg. Chem. 2012, 51, 5299.
[56] O. Mayasree, Y. Cui, A. Assoud, H. Kleinke, Inorg. Chem. 2010, 49, 6518.
[57] S. Jana, G. Panigrahi, B. Tripathy, S. K. Malladi, M. K. Niranjan, J. Prakash, J. Solid State Chem. 2022, 308, 122914.
[58] A. Assoud, C. R. Sankar, H. Kleinke, Solid State Sci. 2014, 38, 124.
[59] T. J. Boerner, S. Deems, T. R. Furlani, S. L. Knuth, J. Towns, in Practice and Experience in Advanced Research Computing (PEARC '23), Portland, OR, USA, ACM, New York, NY, USA July 2023, p. 4.
[60] A. Abudurusuli, K. Wu, S. Pan, New J. Chem. 2018, 42, 3350.

Manuscript received: February 25, 2025
Revised manuscript received: April 8, 2025
Version of record online: May 2, 2025

